

The effect of an expanding universe on massive objects

Roshina Nandra^{1,2*}, Anthony N. Lasenby^{1,2*} and Michael P. Hobson^{1*}

¹*Astrophysics Group, Cavendish Laboratory, JJ Thomson Avenue, Cambridge CB3 0HE, U.K.*

²*Kavli Institute for Cosmology, c/o Institute of Astronomy, Madingley Road, Cambridge CB3 0HA, U.K.*

Accepted —. Received —; in original form 24 September 2018

ABSTRACT

We present some astrophysical consequences of the metric for a point mass in an expanding universe derived in Nandra, Lasenby & Hobson, and of the associated invariant expression for the force required to keep a test particle at rest relative to the central mass. We focus on the effect of an expanding universe on massive objects on the scale of galaxies and clusters. Using Newtonian and general-relativistic approaches, we identify two important time-dependent physical radii for such objects when the cosmological expansion is accelerating; these radii are found to be insensitive to relativistic effects. The first radius, r_F , is that at which the total radial force on a test particle is zero, which is also the radius of the largest possible circular orbit about the central mass m and where the gas pressure and its gradient vanish. The second radius, r_S , is that of the largest possible stable circular orbit, which we interpret as the theoretical maximum size for an object of mass m . The radius r_S is typically smaller than r_F by a factor ~ 1.6 . In contrast, for a decelerating cosmological expansion, no such finite radii exist. Assuming a cosmological expansion consistent with a Λ CDM concordance model, at the present epoch we find that these radii put a sensible constraint on the typical sizes of both galaxies and clusters at low redshift. For galaxies, we also find that these radii agree closely with zeroes in the radial velocity field in the neighbourhood of nearby galaxies, as inferred by Peirani & Pacheco from recent observations of stellar velocities. We then consider the future effect on massive objects of an accelerating cosmological expansion driven by phantom energy, for which the universe is predicted to end in a ‘Big Rip’ at a finite time in the future at which the scale factor and the Hubble parameter become singular. In particular, we present a novel way of calculating the time prior to the Big Rip that an object of a given mass and size will become gravitationally unbound.

Key words: gravitation – cosmology: theory – galaxies: evolution – galaxies: kinematics and dynamics – galaxies: general – galaxies: clusters: general

1 INTRODUCTION

In Nandra, Lasenby & Hobson (2011) (hereafter NLH1), we considered the effect of a massive object on an expanding universe by deriving the metrics that describe a point mass in spatially-flat and spatially-curved cosmologies. In particular, we derived a general invariant expression for the force required to keep a test particle at rest relative to the point mass. Conversely, one would expect cosmological expansion to have a significant effect on the dynamics of massive objects. In this paper, we investigate this effect for objects on the scale of galaxies and clusters.

Considering the radial motion of a test particle in a

spatially-flat expanding universe, we showed in NLH1 that, in the Newtonian limit, the radial force F per unit mass at a distance r from a point mass m is given by

$$F = -\frac{m}{r^2} - q(t)H^2(t)r, \quad (1)$$

where $H(t) \equiv R'(t)/R(t)$ is the Hubble parameter, $q(t) = -H'(t)/H^2(t) - 1$ is the deceleration parameter, $R(t)$ is the universal scale factor and primes denote derivatives with respect to the cosmic time t .¹ Thus, the force consists of the usual time-independent $1/r^2$ component due to the central mass and a time-dependent cosmological component proportional to r that is directed outwards (inwards) when the cosmological expansion is accelerating (decelerating); see also Davis, Lineweaver & Webb (2003). For the currently

* E-mail: rn288@mrao.cam.ac.uk (RN); a.n.lasenby@mrao.cam.ac.uk (ANL), mph@mrao.cam.ac.uk (MPH)

¹ We will work in natural units throughout, so that $c = G = 1$.

favoured spatially-flat Λ CDM cosmology, the cosmological force reverses direction at redshift $z \approx 0.67$.

We will consider this general case (and its general-relativistic extension) in due course, but the main physical effects of the present-day accelerating cosmological expansion on the dynamics of massive objects can be illustrated by considering the special case of a de Sitter universe, which contains no cosmological matter fluid (or radiation), but only dark energy in the form of a non-zero cosmological constant Λ . In this case, the Hubble parameter and, hence, the deceleration parameter become time-independent and are given by $H = \sqrt{\Lambda/3}$ and $q = -1$. Thus, the force (1) also becomes time-independent and reads

$$F = -\frac{m}{r^2} + \frac{1}{3}\Lambda r. \quad (2)$$

The time-independence of this expression is related to the well-known (but curious) fact that the presence of a pure non-zero cosmological constant can be treated mathematically in a completely static manner. As we will discuss in Section 4, even in the full general-relativistic case, the metric for a point mass embedded in an expanding de Sitter cosmological background is connected by a simple coordinate transformation to the standard Schwarzschild–de Sitter metric, which is static. Thus, in this special case, this correspondence unburdens us from the need to include directly the expanding cosmological background and allows us to consider simply the static case of a point mass in the presence of a non-zero cosmological constant. Indeed, (2) is easily obtained by considering directly the Newtonian limit of the Einstein field equations with $\Lambda \neq 0$ in this case (McCauley 1997). Moreover, this correspondence enables us to generalise straightforwardly to spatially finite (i.e. non-pointlike) spherically-symmetric massive objects. In the Newtonian limit, for example, (2) is replaced simply by

$$F = -\frac{M(r)}{r^2} + \frac{1}{3}\Lambda r, \quad (3)$$

where $M(r)$ is the total mass of the object contained within the radius r . If the object has the radial density profile $\rho(r)$, then $M(r) = \int_0^r 4\pi\bar{r}^2\rho(\bar{r})d\bar{r}$.

Although the de Sitter background is not an accurate representation of our universe, the standard cosmological model is dominated by dark-energy in a form consistent with a simple cosmological constant, which is driving the current observed acceleration of the universal expansion (Straumann 2002; Hubble 1929; Riess et al. 2004; Kratochvil et al. 2004; Garnavich et al. 1998). It is therefore of interest to consider the astrophysical (as opposed to cosmological) consequences of a non-zero Λ , which has previously been considered only in the context of growth of structure analyses (Lahav et al. 1991).

Even in the simple Newtonian case, embodied by the force expression (3), we see immediately that there is an obvious, but profound, difference between the cases $\Lambda = 0$ and $\Lambda \neq 0$. In the former, the force on a constituent particle of a galaxy or cluster (say) is attractive for all values of r and tends gradually to zero as $r \rightarrow \infty$ (for any sensible radial density profile). In the latter case, however, the force on a constituent particle (or equivalently its radial acceleration) *vanishes* at the *finite* radius r_F which satisfies $r_F = [3M(r_F)/\Lambda]^{1/3}$, beyond which the net force becomes

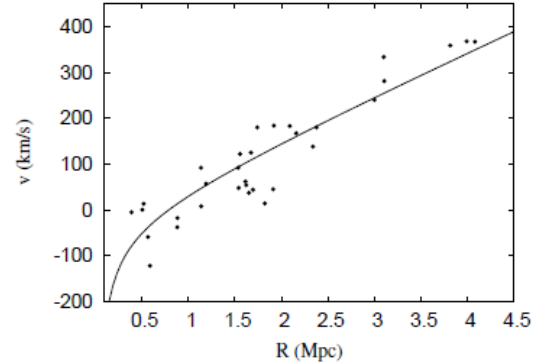


Figure 1. Radial-velocity versus distance of stars in the M81 group, which has a mass of $9.2 \times 10^{11} M_{\odot}$, and the best-fit line (4) (reproduced from Peirani & Pacheco 2008).

repulsive. This suggests that a non-zero Λ should set a *maximum size*, dependent on mass, for galaxies and clusters.

Some observational evidence for this suggestion has been reported by Peirani & Pacheco (2005, 2008), who analysed the radial velocities of stars in the neighbourhood of a number of nearby galaxies, including M83, M81, IC 342 and NGC 253, by collating a number of unrelated observational studies (Karachentsev 2005). Note that all these galaxies lie at very low redshift ($z \sim 10^{-4}$ – 10^{-3}). The data for M81 are shown in Fig. 1. To obtain the best-fit line for each galaxy, it was modelled as a system consisting of low-mass satellites sitting within expanding shells around a dominant core of mass m . Such an approach had already been proposed by Lynden-Bell (1981) and Sandage (1986) and is based on the Lemaître-Tolman (LT) model (Lemaître 1933; Tolman 1934). One essentially begins with the simple Newtonian expression (3) for the radial acceleration from which an expression for the radial velocity can be calculated, containing initially unknown constants. Obtaining an analytical expression in the case of a non-zero cosmological constant is problematic, so Peirani & Pacheco instead found a numerical solution to the relativistic LT model, valid for $z \approx 0$:

$$v_{\text{radial}}(r) = -\frac{0.976}{r^n} \left(\frac{m}{H_0^2} \right)^{\frac{n+1}{3}} + 1.377H_0 r, \quad (4)$$

where $n = 0.627$ and H_0 is the present-day Hubble constant. This relation appears to fit the data extremely well, and highlights the existence of a well-defined ‘cut-off’ radius, depending on the galaxy mass, at which the radial velocity is zero, separating bound and unbound material. We see that this radius is ~ 0.8 Mpc for M81. This is around 3 times the typical extent of ~ 0.26 Mpc quoted in Klypin, Zhao & Somerville (2002) for the Milky Way, which has a similar mass to M81.

The numerical analysis of Peirani & Pacheco (2005, 2008) is based on radial velocities, and it relies on observational data to fit values to the initially unknown constants. To avoid this reliance, in this paper we consider instead test particles in circular orbits about the central mass, which is also simpler and potentially more representative of the trajectories of constituent particles of galaxies and clusters. From (3), in the Newtonian limit, the speed of a particle in

a circular orbit of radius r is given simply by

$$v(r) = \sqrt{\frac{M(r)}{r} - \frac{1}{3}\Lambda r^2}, \quad (5)$$

from which it is clear that no circular orbit can exist beyond the radius r_F . A second physically significant radius r_S is that of the largest *stable* circular orbit, which lies somewhat within r_F , as we will discuss in Section 4. Indeed, the latter provides a more physically meaningful limit on the maximum sizes of galaxies and clusters.

The existence and stability of circular orbits around a central mass in an expanding universe have been considered previously by Sussman & Hernandez (2003), Nowakowski, Sanabria & Garcia (2002), Balaguera-Anol3nez, B3hmer & Nowakowski (2005) and Nowakowski & Balaguera-Anol3nez (2006). Some details of their work are given in Section 4.4. In particular, they assumed a de Sitter cosmological background and treated the central mass as pointlike. In this paper, we will relax both these assumptions, although not simultaneously.

The overall structure of this paper is as follows. In Section 2, we perform a circular velocity analysis based on the simple Newtonian expression (5) applied to two assumed radial density profiles $\rho(r)$ for the central object: a decaying exponential and an NFW profile (Navarro, Frenk & White 1996; Matos, Nu3nez & Sussman 2004). We compare our results with the radial velocity analysis of Peirani & Pacheco (2005, 2008) and also derive an analytical expression for the pressure profile. In Section 3, we extend our analysis to the general-relativistic case, for which we obtain an analytical circular velocity expression in the linearised case and employ a numerical approach when considering the full Einstein equations. In the latter case, we again consider the pressure profile in the central object. In Section 4, we remove our assumption of a de Sitter background cosmology and consider the currently-favoured Λ CDM model with $\Omega_{m,0} = 0.3$ and $\Omega_{\Lambda,0} = 0.7$, albeit at the cost of having to model the central object as a point mass. By comparing with the de Sitter background model in this case we thus obtain ‘correction’ factors that may be applied to our earlier results for the radius r_F . We also obtain an expression for the radius r_S of the largest stable circular orbit. In Section 5, we investigate the more speculative scenario that the expansion of the universe is driven by phantom energy, leading to the prediction that the universe will end in a ‘Big Rip’ (Caldwell, Kamionkowski & Weinberg 2009). In particular, we use our force expression to find the times prior to the Big Rip at which objects of a given mass and size would be expected to become unbound. Our conclusions are presented in Section 6.

Finally, we note that in this paper we model galaxies/clusters as being composed of a single ‘phenomenological’ fluid, with a single overall density profile and a single associated (effective) pressure required for stability; this is explained in more detail in the next section. This avoids the complexity of an explicit non-linear multi-fluid treatment, whereby one would separate the fluid into its baryonic and dark matter components. The analyses we perform in this work are therefore designed to highlight general features, and only indicate the existence and approximate locations of the radii r_F and r_S .

Quantity	Galaxies	Clusters
r_0 (kpc)	3	500
r_T (Mpc)	0.26	5
$M(r_T)$ (M_\odot)	10^{12}	10^{15}

Table 1. Summary of the values assumed in our modelling of galaxies and clusters. Note that the values for galaxies correspond to the virial radius/mass of the Milky Way, as given in Table 2 of Klypin, Zhao & Somerville (2002).

2 NEWTONIAN DE SITTER ANALYSIS

We first adopt the simple Newtonian expression (5) for the circular velocity. To plot the circular velocity function we must choose a form for the density distribution. The central massive object is modelled as a total ‘effective’ fluid, made up of two components: baryonic gas and dark matter. It is assumed that both components follow a common density distribution (up to an overall normalisation), such that the total density $\rho(r) = \rho_g(r) + \rho_{dm}(r)$, where $\rho_g(r) = f_g \rho_{dm}(r)/(1 - f_g)$ and $f_g = \rho_g(r)/\rho(r)$ is the uniform gas fraction throughout the object. Specifically, assuming spherical symmetry, we consider two model radial profiles. The first is a decaying exponential

$$\rho(r) = \rho_0 e^{-\frac{r}{r_0}}, \quad (6)$$

where r_0 is a characteristic physical scale of the object and ρ_0 is its central density. The second is a Navarro, Frenk and White (NFW) profile (Navarro, Frenk & White 1996; Matos, Nu3nez & Sussman 2004)

$$\rho(r) = \frac{\rho_0 r_0}{r \left(1 + \frac{r}{r_0}\right)^2}, \quad (7)$$

where r_0 is again a characteristic physical scale, but ρ_0 is a characteristic density in this case, since the central density of (7) is infinite. In each case, we fix the constant r_0 directly and then determine ρ_0 by assuming the mass $M(r_T)$ inside a ‘typical’ size r_T for low-redshift galaxies and clusters as listed in Table 1. We also assume the value of the cosmological constant to be $\Lambda = 10^{-35} \text{ s}^{-2}$, which is consistent with observations (Carmeli & Kuzmenko 2001; Carroll 2001; Weinberg 1989; Krauss 2003).

The resulting Newtonian circular velocity (5) is plotted in Fig. 2. As expected, in each case the circular velocity, and hence the radial force, falls to zero at a finite radial distance from the centre of the object. This is in sharp contrast to the situation when $\Lambda = 0$ (also plotted in Fig. 2), in which case there is no definite cut-off radius. Although, for $\Lambda \neq 0$, the radial force vanishes at r_F , this marks the position of an unstable equilibrium, since any radial displacement of a test particle would move it to a region where either the gravitational or cosmological force dominates (Faraoni & Jacques 2007). We note that for the galaxy and the cluster, the cut-off radius r_F is smaller for the exponential radial density profile than for the NFW profile. Table 2 gives the cut-off radii r_F for the modelled objects.

One may also use the plots in Fig. 2 to read off the maximum circular velocities v_{\max} , which clearly lie close to the centres of the modelled objects. Using a decaying exponential profile (6), for a typical galaxy $v_{\max} \sim 530 \text{ km/s}$, and for a typical cluster $v_{\max} \sim 1280 \text{ km/s}$. Since the to-

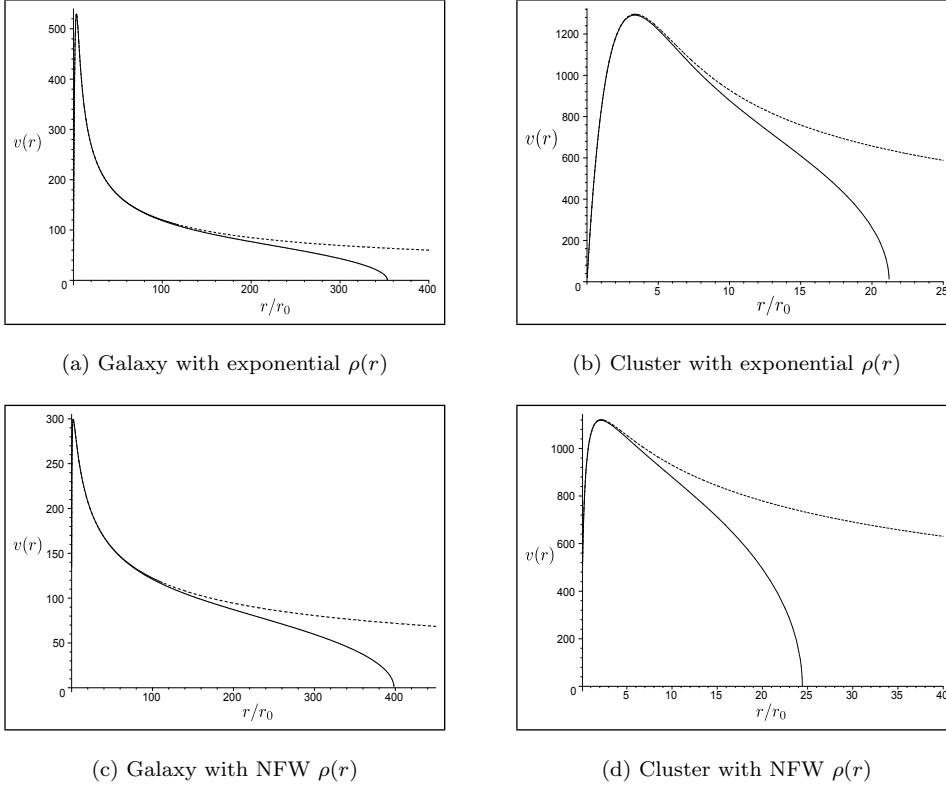


Figure 2. Circular velocity $v(r)$, in km/s, obtained from the Newtonian expression (5) assuming $\Lambda = 10^{-35} \text{ s}^{-2}$ (solid line) and $\Lambda = 0$ (dotted line).

	Galaxies	Clusters
Exponential $\rho(r)$	1.06	10.5
NFW $\rho(r)$	1.20	12.0

Table 2. The distance r_F (in Mpc) at which the total radial force and circular velocities vanish for ‘galaxies’ and ‘clusters’, using a Newtonian de Sitter analysis and the values for parameters given in Table 1. Note that the r_F values are read from the plots in Fig. 2.

tal effective fluid is largely dominated by dark matter, an NFW profile (7) is likely to be more realistic. This leads to $v_{\text{max}} \sim 300 \text{ km/s}$ for a typical galaxy and $v_{\text{max}} \sim 1120 \text{ km/s}$ for a typical cluster. Indeed in this case the maximum circular velocity for a galaxy is only about 1.3 times higher than that found by Klypin, Zhao & Somerville (2002).

Having laid down two possible density profiles, we may find the associated pressure $p(r)$ required to keep the overall fluid stable. This too is made up of two components: an ordinary pressure associated with the gas $p_g(r)$ and an effective pressure associated with the dark matter $p_{\text{dm}}^{\text{eff}}(r)$. The latter arises when the motions of dark matter particles have suffered phase-mixing and relaxation, such that their velocities are randomised and the object is virialised, as explained by Lynden-Bell (1967) and more recently by Binney & Tremaine (2008). The total pressure is then given by $p(r) = p_g(r) + p_{\text{dm}}^{\text{eff}}(r)$.

The controlling equation for gas in hydrostatic equilib-

rium is

$$\frac{d}{dr}(p_g(r)) = -\rho_g(r) \frac{d\Phi(r)}{dr}, \quad (8)$$

where $\Phi(r)$ is the gravitational potential. The corresponding equation for the dark matter, modelled as composed of collisionless particles which have achieved dynamical equilibrium, is the Jeans equation,

$$\frac{d}{dr}(\rho_{\text{dm}}(r)\sigma_r^2(r)) = -\rho_{\text{dm}}(r) \frac{d\Phi(r)}{dr}, \quad (9)$$

where $\sigma_r^2(r)$ is the radial velocity dispersion (Tormen, Bouchet & White 1997). Note that we have ignored a possible ‘softening’ correction by assuming an isotropic velocity distribution, which follows naturally from our assumption of full spherical symmetry. Comparing (9) with (8), one can see that the two equations are in identical form, and therefore that the effective pressure of the dark matter is given by

$$p_{\text{dm}}^{\text{eff}}(r) = \rho_{\text{dm}}(r)\sigma_r^2(r). \quad (10)$$

We assume that the only interaction between the gas and the dark matter is gravitational, so $\Phi(r)$ corresponds to the total gravitational potential. In the presence of a non-zero cosmological constant, for a fixed total mass $M(r)$ within a radius r , the gravitational potential is $\Phi(r) = -\int_r^\infty (M(r')/r'^2) dr' - (1/6)\Lambda r^2$. Thus, adding the two equations (8) and (9) together leads to the standard Newtonian equation for hydrostatic equilibrium, namely

$$\frac{dp(r)}{dr} = -\frac{\rho(r)[M(r) - \frac{1}{3}\Lambda r^3]}{r^2}. \quad (11)$$

For $\Lambda = 0$, we see immediately that $dp(r)/dr$ is always negative, tending to zero as $r \rightarrow \infty$. For $\Lambda \neq 0$, however, the

behaviour is radically different and using (5) we see that the pressure profile has a minimum precisely at $r = r_F$.

For brevity, we will consider only the (possibly more realistic) NFW profile. With an appropriate choice of boundary condition, one may in fact obtain an analytical form for $p(r)$ (albeit rather unwieldy) for general Λ , which we believe has not been reported previously. The boundary condition in both the $\Lambda = 0$ and $\Lambda \neq 0$ cases is that the pressure itself vanishes at the point where $dp(r)/dr = 0$. Thus, for $\Lambda = 0$, one has $p(r) \rightarrow 0$ as $r \rightarrow \infty$, whereas for $\Lambda \neq 0$ one requires $p(r_F) = 0$. In the latter case, one thus has yet another physically important interpretation of the radius $r = r_F$. One finds that the pressure profile is given by

$$\begin{aligned}
 p(r) = & -\frac{4\pi\rho_0^2 r_0^2 \ln\left(1 + \frac{r}{r_0}\right)}{1 + \frac{r}{r_0}} - \frac{12\pi\rho_0^2 r_0^2}{1 + \frac{r}{r_0}} \\
 & + 12\pi\rho_0^2 r_0^2 \operatorname{dilog}\left(1 + \frac{r}{r_0}\right) + 6\pi\rho_0^2 r_0^2 \left[\ln\left(1 + \frac{r}{r_0}\right)\right]^2 \\
 & - 2\pi\rho_0^2 r_0^2 \ln\left(\frac{r}{r_0}\right) - \frac{2\pi\rho_0^2 r_0^3}{r} + \frac{2\pi\rho_0^2 r_0^4 \ln\left(1 + \frac{r}{r_0}\right)}{r^2} \\
 & - \frac{8\pi\rho_0^2 r_0^3 \ln\left(1 + \frac{r}{r_0}\right)}{r} + 2\pi\rho_0^2 r_0^2 \ln\left(1 + \frac{r}{r_0}\right) \\
 & - \frac{2\pi\rho_0^2 r_0^2}{\left(1 + \frac{r}{r_0}\right)^2} - \frac{\Lambda\rho_0 r_0^2}{3\left(1 + \frac{r}{r_0}\right)} + C, \quad (12)
 \end{aligned}$$

where $\operatorname{dilog}(1+r) = \int_0^{1+r} \frac{\ln(t)}{1-t} dt$; it is worth noting that $\operatorname{dilog}(1+r) \rightarrow -\frac{1}{2}[\ln r]^2 - \frac{1}{6}\pi^2$ as $r \rightarrow \infty$. The constant of integration C is set by the above boundary condition on $p(r)$. For the $\Lambda = 0$ case, it has the analytical value $C = 2\pi^3 r_0^2 \rho_0^2$, whereas for $\Lambda \neq 0$ its value was found numerically.

Rather than the pressure profile $p(r)$ itself, of more interest, perhaps, is the ratio $p(r)/\rho(r)$. Assuming a perfect gas law and mean molecular weight of $m_p/2$, we can relate this numerically to a temperature, in K, via

$$T(r) = \frac{m_p}{2k_B} \left[\frac{p(r)}{\rho(r)} \right]_{\text{SI}} = \frac{m_p c^2}{2k_B} \left[\frac{p(r)}{\rho(r)} \right]_{\text{nat}}, \quad (13)$$

where m_p is the proton mass, k_B is Boltzmann's constant and the ratio $p(r)/\rho(r)$ may be expressed in Nm/kg (SI units), or in natural units which we mostly adopt in this paper. This temperature profile is, in fact, that of the gas, $T(r) = T_g(r)$. This follows immediately from our assumption that the gas fraction f_g is uniform throughout the galaxy/cluster, in which case, using (8) and (9) respectively, one has

$$\frac{p}{\rho} = \frac{p_g}{\rho_g} = \frac{p_{\text{dm}}^{\text{eff}}}{\rho_{\text{dm}}}. \quad (14)$$

For $\Lambda = 0$, the temperature profile (13) can be expressed in a universal scale-free form as

$$\begin{aligned}
 T(x) = & \frac{\pi G \rho_0 r_0^2 m_p}{k_B x} \{ (x^3 - 5x^2 - 3x + 1)(1+x) \ln(1+x) \\
 & + x^2(1+x)^2 [6 \operatorname{dilog}(1+x) + 3(\ln(1+x))^2 - \ln x] \\
 & + x[\pi^2 x^3 + (2\pi^2 - 7)x^2 + (\pi^2 - 9)x - 1] \}, \quad (15)
 \end{aligned}$$

where $x \equiv r/r_0$. However, for $\Lambda \neq 0$, the term in Λ in (12) breaks scale invariance, and we can no longer write the temperature profile in this universal way.

The peak in the temperature profile (15) occurs at $x = x_m \approx 0.76$, and in terms of x_m one can show analytically that the peak temperature has the value

$$T_{\text{max}} = \frac{x_T(1+x_T)[(1+x_m)\ln(1+x_m) - x_m]}{2x_m(1+3x_m)[(1+x_T)\ln(1+x_T) - x_T]} \frac{GM_T m_p}{r_T k_B}, \quad (16)$$

where, as above, M_T is the object's mass at radius r_T , and $x_T = r_T/r_0$. Since the total gravitational potential energy of the object is $\sim GM_T^2/r_T$, and the kinetic energy of the constituent particles is $\sim (M_T/m_p)k_B T$, it follows that our expression for T_{max} (16) in fact corresponds to an analytical factor times the virial temperature. For the 'typical' values of r_T and r_0 for a cluster given in Table 1, $x_T = 10$ and we obtain

$$T_{\text{max}} \approx 0.32 \frac{GM_T m_p}{r_T k_B} \approx 3.3 \times 10^7 \text{ K} \quad (17)$$

or $T_{\text{max}} \sim 2.8 \text{ keV}$. We may compare this calculated value against the virial temperatures of similar sized clusters as inferred from X-ray data and simulations; indeed our value for T_{max} is in close agreement with the simulations of Roncarelli et al. (2006) and lies within the range found in X-ray observations by Vikhlinin et al. (2006).

Note that for a galaxy with the parameters in Table 1 we can calculate that $T_{\text{max}} \approx 2.4 \times 10^6 \text{ K}$. There has been long dispute about whether a component of hot halo gas exists for galaxies, but recent X-ray observations, summarised in Crain et al. (2010), do support such a component. In fact the temperature of the hot gas halo of the Milky Way itself (the mass and size parameters of which were used in Table 1) has recently been measured (Henley et al. 2010) and lies in the range $1.8\text{--}2.4 \times 10^6 \text{ K}$, in good agreement with our calculated figure. Of course the behaviour of the gas in the inner regions of galactic haloes and clusters is more or less independent of the effects of Λ or universe expansion (see Fig. 3, where the effects of Λ only become perceptible to the right of the peak in temperature), but we mention these details, and corroborating observations, to show that our model does work sensibly in these inner regions, and therefore plausibly reflects reality in the outer regions as well.

Turning then to the broader features of the temperature profiles, for $\Lambda = 0$, the ratio $p(r)/\rho(r)$ is plotted in Fig. 3 for a galaxy and a cluster (dotted lines), and exhibits an initial increase away from the centre, to the peak just described, and then a gradual tailing off as $r \rightarrow \infty$. This should be compared with the corresponding temperature profiles shown in Fig. 3 for $\Lambda \neq 0$ (solid lines). We see that the introduction of a non-zero Λ has a similar effect on the temperature profile $p(r)/\rho(r)$ as it had on the circular velocity profile $v(r)$, namely it introduces a definite cut-off radius at which the temperature (and pressure) vanish. Since both $p(r)$ and $dp(r)/dr$ vanish at $r = r_F$, the temperature profile $p(r)/\rho(r)$ also vanishes there.

Finally, rearranging equation (10) and employing the equivalence of the ratios given by equation (14), it is found that $p(r)/\rho(r)$ is also related to the velocity dispersion of the dark matter particles through

$$\sigma_r^2(r) = c^2 \left[\frac{p(r)}{\rho(r)} \right]_{\text{nat}} = \frac{2k_B T(r)}{m_p}, \quad (18)$$

where the right-most-side is obtained using (13). Since this

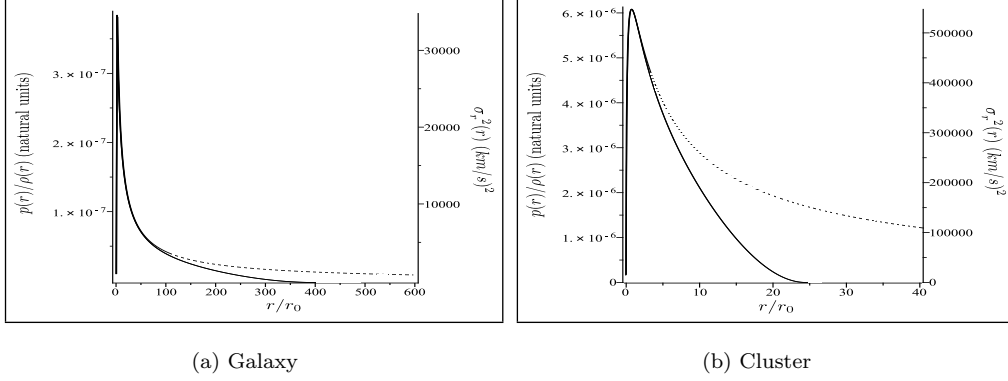


Figure 3. Temperature profiles $p(r)/\rho(r)$ for a galaxy and a cluster with NFW density profiles obtained using Newtonian theory assuming $\Lambda = 10^{-35} \text{ s}^{-2}$ (solid line) and $\Lambda = 0$ (dotted line). Note that the solid lines actually rise again beyond their minima, but since these results are unphysical we have omitted them in the plots.

virial relation is independent of the mass of the dark matter particles, it is expected to be applicable to all constituents of the overall object which behave like collisionless particles in the gravitational potential. Using it to calculate the peak velocity dispersion of galaxies within a cluster, using the peak temperature given by (17) we obtain $\sigma_{\text{max}} \approx 740 \text{ km/s}$, which is of the same order of magnitude as the averages found by Fleenor et al. (2006). The overall scale for $\sigma_r^2(r)$ through a whole galaxy/cluster is shown on a second vertical axis in Fig. 3.

Even from this simple Newtonian analysis, in which the expanding universe is modelled rather crudely as a de Sitter background, comparing Tables 1 and 2 we see that $r_F \sim 2r_T$ for clusters and $r_F \sim 4r_T$ for galaxies, which is very encouraging. In addition, for galaxies the values of r_F are also in broad agreement with the ‘cut-off’ radius at which the radial velocity field vanishes in the neighbourhood of M81, as found observationally by Peirani & Pacheco (2005, 2008) (see Fig. 1). Given the success of our basic Newtonian approach, in the next section we investigate the effects of general-relativistic corrections on our analysis.

3 GENERAL-RELATIVISTIC DE SITTER ANALYSIS

We now extend our analysis to include general-relativistic effects to obtain a more accurate estimate of the radius r_F for galaxies and clusters and also to study further the pressure profile in such objects. We again assume a de Sitter background universe.

Einstein’s field equations with the inclusion of a non-zero cosmological constant are

$$R_{\mu\nu} - \frac{1}{2}g_{\mu\nu}R = \kappa T_{\mu\nu} + \Lambda g_{\mu\nu}, \quad (19)$$

where $\kappa = 8\pi$, $T_{\mu\nu}$ is the matter energy-momentum tensor, $R_{\mu\nu} \equiv R^{\rho}{}_{\mu\rho\nu}$ and R denote the Ricci tensor and scalar respectively, and we adopt the metric signature $(+, -, -, -)$. We use two approaches to solve these equations and find an expression for the speed $v(r)$ of a test particle in a circular orbit of coordinate radius r about a massive object, as measured by a stationary observer at that radius. First, we linearise the field equations, which necessitates assuming a pressureless fluid within the massive object, but yields an

analytical form for $v(r)$. Second, we consider the full non-linear field equations and again include the effect of pressure; this requires a numerical solution to obtain $v(r)$ and the fluid pressure profile $p(r)$ within the massive object. In both cases, we restrict the central object to be spherically symmetric and again denote $M(r) = \int_0^r 4\pi\bar{r}^2\rho(\bar{r})d\bar{r}$.

3.1 Linearised field equations

The linearised field equations, with their attendant Lorenz gauge constraint, are often written in the form

$$\begin{aligned} \square^2 \bar{h}^{\mu\nu} &= -2(\kappa T^{\mu\nu} + \Lambda \eta^{\mu\nu}), \\ \partial_\mu \bar{h}^{\mu\nu} &= 0, \end{aligned} \quad (20)$$

where $g_{\mu\nu} = \eta_{\mu\nu} + h_{\mu\nu}$, $\eta_{\mu\nu}$ is the Minkowski metric of flat spacetime and $h_{\mu\nu}$ is a small perturbation (Hobson, Efstathiou & Lasenby 2006). Also the d’Alembertian operator is defined by $\square^2 \equiv \partial_\sigma \partial^\sigma$, $\bar{h}_{\mu\nu} \equiv h_{\mu\nu} - \frac{1}{2}\eta_{\mu\nu}h$ and $h \equiv h^\sigma{}_\sigma$. One must realise, however, that this form represents the field equations specifically in Cartesian coordinates (x, y, z) , whereas we wish to work in spherical polar coordinates (r, θ, ϕ) . In general one may interpret the linearised field equations as describing a rank-2, symmetric ‘gravitational field’ $h_{\mu\nu}$ in Minkowski spacetime, so to convert them (and the Lorenz gauge condition) to curvilinear coordinates in the same spacetime one simply makes the replacements $\eta_{\mu\nu} \rightarrow \gamma_{\mu\nu}$ and $\partial_\mu \rightarrow \nabla_\mu$ throughout (Misner, Thorne & Wheeler 1973). Here $\gamma_{\mu\nu}$ is the Minkowski metric in curvilinear coordinates and ∇_μ is the covariant derivative defined in terms of $\gamma_{\mu\nu}$, namely

$$\begin{aligned} \nabla_\mu \bar{h}^{\mu\nu} &= \partial_\mu \bar{h}^{\mu\nu} + \Gamma^\mu_{\rho\mu} \bar{h}^{\rho\nu} + \Gamma^\nu_{\rho\mu} \bar{h}^{\mu\rho}, \\ \Gamma^\nu_{\rho\mu} &= \frac{1}{2}\gamma^{\nu\sigma}(\partial_\rho \gamma_{\sigma\mu} + \partial_\mu \gamma_{\rho\sigma} - \partial_\sigma \gamma_{\rho\mu}). \end{aligned} \quad (21)$$

Working in spherical polar coordinates we specifically use $\gamma_{\mu\nu} = \text{diag}(1, -1, -r^2, -r^2 \sin^2 \theta)$.

3.1.1 Tetrad method

We now obtain a solution to the linearised field equations (20) for a static, spherically-symmetric, pressureless mass distribution $M(r)$ using a tetrad-based approach. This method will also prove useful in solving the full non-linear field equations and provides consistency with our approach

in NLH1. Note that a full explanation behind this method is given in NLH1, so we skip straight to the tetrad definitions here.

For a spherically-symmetric system in the linearised case, we may assume a form for the tetrads obtained simply by perturbing those for the flat Minkowski metric in spherical polar coordinates by unknown functions $a(r)$, $b(r)$ and $c(r)$:

$$\begin{aligned} e_0^0 &= 1 + a(r), & e_0^0 &= 1/(1 + a(r)), \\ e_1^1 &= 1 + b(r), & e_1^1 &= 1/(1 + b(r)), \\ e_2^2 &= (1 + c(r))/r, & e_2^2 &= r/(1 + c(r)), \\ e_3^3 &= (1 + c(r))/(r \sin \theta), & e_3^3 &= r \sin \theta / (1 + c(r)). \end{aligned} \quad (22)$$

For a test particle with general four-velocity \mathbf{u} , the components in the coordinate basis $u^\mu = [\dot{t}, \dot{r}, \dot{\theta}, \dot{\phi}]$ are related to those in the tetrad frame (denoted by hats) by $u^\mu = e_i^\mu \hat{u}^i$, where dots denote derivatives with respect to the particle's proper time τ . Thus, we see that for a particle (or observer) at rest in the tetrad frame, so that $\hat{u}^i = [1, 0, 0, 0]$, then $\dot{t} = 1 + a(r)$ and $\dot{r} = \dot{\theta} = \dot{\phi} = 0$. Therefore our tetrad frame defines the local laboratory of an observer at fixed spatial coordinates. Moreover, the three spacelike tetrad unit vectors \hat{e}_i ($i = 1, 2, 3$) lie in the same directions as the spatial coordinate basis vectors e_μ ($\mu = 1, 2, 3$).

The line-element corresponding to the tetrads (22) is given by

$$ds^2 = \left[\frac{1}{1 + a(r)} \right]^2 dt^2 - \left[\frac{1}{1 + b(r)} \right]^2 dr^2 - \left[\frac{r}{1 + c(r)} \right]^2 d\Omega^2. \quad (23)$$

where $d\Omega^2 = d\theta^2 + \sin^2 \theta d\phi^2$. To first-order in the perturbation functions, we thus have

$$h^{\mu\nu} = \text{diag}[-2a(r), 2b(r), 2c(r)/r^2, 2c(r)/(r^2 \sin^2 \theta)]. \quad (24)$$

Substituting this form into the field equations and Lorenz gauge constraint (20) (appropriately modified to spherical polar coordinates) and taking the energy-momentum tensor to be that of a perfect fluid with zero pressure, yields the coupled differential equations (momentarily dropping the explicit dependencies on r for brevity)

$$\begin{aligned} a_2 - b_2 - 2c_2 + \frac{2}{r}(a_1 - b_1 - 2c_1) + 16\pi\rho + 2\Lambda &= 0, \\ a_2 - b_2 + 2c_2 + \frac{2}{r}(a_1 - b_1 + 2c_1) + \frac{8}{r^2}(b - c) - 2\Lambda &= 0, \\ a_2 + b_2 + \frac{2}{r}(a_1 + b_1) - \frac{4}{r^2}(b + c) - 2\Lambda &= 0, \end{aligned} \quad (25)$$

where $a_1 \equiv da(r)/dr$, $a_2 \equiv d^2a(r)/dr^2$, and similar for the derivatives of $b(r)$ and $c(r)$, and the Lorenz gauge condition becomes

$$-a_1 + b_1 - 2c_1 + \frac{4}{r}(b + c) = 0. \quad (26)$$

Solving these equations for the three unknown functions

$a(r)$, $b(r)$ and $c(r)$ gives

$$\begin{aligned} a(r) &= - \int \frac{I_1(r) + C_1}{r^2} dr + C_2, \\ b(r) &= I_3(r) + C_4, \\ c(r) &= \frac{I_2(r)}{2r^3} + \frac{C_3}{2r^3} - \frac{I_1(r)}{2r} - \frac{C_1}{2r} + I_3(r) - \frac{\Lambda r^2}{2} + C_4, \end{aligned} \quad (27)$$

where we have defined the integral functions

$$\begin{aligned} I_1(r) &= \int [4\pi\rho(r) - \Lambda] r^2 dr \\ I_2(r) &= \int [2rI_1(r) + 2rC_1 + 4\pi\rho(r)r^4 + 3\Lambda r^4] dr \\ I_3(r) &= \int \frac{I_2(r) + C_3}{r^4} dr, \end{aligned} \quad (28)$$

and the C_i ($i = 1, 2, 3, 4$) are constants of integration.

3.1.2 Circular motion in the equatorial plane

We now derive an expression in terms of the tetrads (22) for the speed $v(r)$ of a test particle in a circular orbit of coordinate radius r about the central mass, as measured by an observer at rest at that radius (i.e. the observer defined by our tetrad frame).

In particular, we consider a test particle moving along a circular path ($\dot{r} = 0$) in the equatorial plane ($\theta = \pi/2$). For such a particle, the components of the four-velocity in the tetrad frame may be written

$$\hat{u}^i = [\cosh \psi(\tau), 0, 0, \sinh \psi(\tau)], \quad (29)$$

where $\psi(\tau)$ is the particle's rapidity in this frame, which may, in general, be a function of the particle's proper time τ . The particle's 3-speed, or circular velocity, v in this frame is simply $v = \hat{u}^3/\hat{u}^0 = \tanh \psi$.

One may obtain an expression for v in terms of the tetrads (22) most simply by using the geodesic equations in the tetrad frame directly, which read (see NLH1)

$$\hat{u}^i + \omega^i_{jk} \hat{u}^j \hat{u}^k = 0, \quad (30)$$

where the spin-connection ω^i_{jk} is given by

$$\begin{aligned} \omega_{ijk} &= \frac{1}{2}(c_{ijk} + c_{jki} - c_{kij}), \\ c^k_{ij} &= e_i^\mu e_j^\nu (\partial_\mu e^k_\nu - \partial_\nu e^k_\mu). \end{aligned} \quad (31)$$

Using the tetrads (22), the non-zero elements of the spin-connection are $\omega^1_{00} = \omega^0_{10}$ and $\omega^1_{22} = \omega^1_{33} = -\omega^2_{12} = -\omega^3_{13}$, where

$$\begin{aligned} \omega^1_{00} &= -\frac{1 + b(r)}{1 + a(r)} \frac{da(r)}{dr}, \\ \omega^1_{22} &= \frac{1 + b(r)}{r(1 + c(r))} \left(r \frac{dc(r)}{dr} - c(r) - 1 \right). \end{aligned} \quad (32)$$

Substituting these expressions into (30) and using (29), one finds that the geodesic equation for $i = 2$ is satisfied identically and the equations for $i = 0, 3$ both reduce to $\dot{\psi} = 0$, which indicates that, as expected, the particle has a constant rapidity, and hence constant 3-speed, in the tetrad frame. Finally, the geodesic equation for $i = 1$ gives

	Exponential $\rho(r)$	NFW $\rho(r)$
C_1	$8\pi\rho_0r_0^3$	$-4\pi\rho_0r_0^3(\ln r_0 + 1)$
C_2	$-4\pi\rho_0r_0^2$	$\frac{1}{6}\Lambda r_0^2 - 4\pi\rho_0r_0^2$
C_3	0	0
C_4	$4\pi\rho_0r_0^2$	$\frac{7}{30}\Lambda r_0^2 + 4\pi\rho_0r_0^2$

Table 3. Values of the constants in the functions $a(r)$, $b(r)$ and $c(r)$ in (27) for each considered density profile.

$\tanh^2\psi = -\omega^1_{00}/\omega^1_{33}$, from which we immediately obtain

$$v(r) = \left[\frac{r(1+c(r))\frac{da(r)}{dr}}{(1+a(r))\left(\frac{dc(r)}{dr} - c(r) - 1\right)} \right]^{\frac{1}{2}}. \quad (33)$$

3.1.3 Results for example radial density profiles

Since the circular velocity is expected to behave sensibly everywhere, the functions $a(r)$, $b(r)$ and $c(r)$ should not diverge at the origin. By considering how their Taylor expansions about $r = 0$ may satisfy this requirement, it is not difficult to solve for the constants C_i ($i = 1, 2, 3, 4$) for a specific radial density profile $\rho(r)$. Expressions for the constants for the exponential profile (6) and the NFW profile (7) are given in Table 3. The resulting circular velocity $v(r)$ profiles are practically identical to those plotted in Fig. 2, and so are not presented separately. This supports our previous results and indicates that linear general-relativistic corrections to the (circular) orbits of test particles are unimportant for massive objects with densities typical of galaxies and clusters, as might be expected. Nonetheless, the analytical results we have derived may prove useful when general-relativistic effects for astronomical extended density distributions become measurable.

3.2 Full non-linear field equations

We now consider the full non-linear Einstein equations and model the massive object as a perfect fluid with some (non-zero) radial pressure profile $p(r)$, as we did for the Newtonian case. To solve the field equations, we again use the tetrad-based method described in NLH1 and employed in the previous section. Fortunately, our task is somewhat simpler for the full field equations than for the linearised equations, since we already considered general, time-dependent, spherically-symmetric systems in this case in NLH1 (see also Lasenby et al. (1998)), which we now summarise.

We have considered a general metric element in terms of three unknown functions $g_1(r, t)$, $g_2(r, t)$ and $f_1(r, t)$,

$$ds^2 = \left(\frac{g_1^2 - g_2^2}{f_1^2 g_1^2} \right) dt^2 + \frac{2g_2}{f_1 g_1^2} dr dt - \frac{1}{g_1^2} dr^2 - r^2 d\Omega^2. \quad (34)$$

We have then shown that, assuming the matter to be a perfect fluid with density $\rho(r, t)$ and $p(r, t)$, Einstein's field equations and the Bianchi identities yield the following re-

lationships between the unknown quantities:

$$\begin{aligned} L_r f_1 &= -G f_1 \Rightarrow f_1 = \exp \left\{ - \int^r \frac{G}{g_1} dr \right\}, \\ L_r g_1 &= F g_1 + \frac{M}{r^2} - \frac{1}{3} \Lambda r - 4\pi r p, \\ L_t g_2 &= G g_1 - \frac{M}{r^2} + \frac{1}{3} \Lambda r - 4\pi r p, \\ L_t M &= -4\pi g_2 r^2 p, \\ L_t \rho &= - \left(\frac{2g_2}{r} + F \right) (\rho + p), \\ L_r M &= 4\pi g_1 r^2 \rho, \\ L_r p &= -G(\rho + p). \end{aligned} \quad (35)$$

Here we have defined two linear differential operators

$$\begin{aligned} L_t &\equiv f_1 \partial_t + g_2 \partial_r, \\ L_r &\equiv g_1 \partial_r, \end{aligned} \quad (36)$$

and the function $F(r, t)$, the radial acceleration, $G(r, t)$, and the intrinsic mass (or energy) interior to r , $M(r, t)$, by

$$\begin{aligned} L_t g_1 &\equiv G g_2, \\ L_r g_2 &\equiv F g_1, \\ M &\equiv \frac{1}{2} r (g_2^2 - g_1^2 + 1 - \frac{1}{3} \Lambda r^2), \end{aligned} \quad (37)$$

where Λ is the cosmological constant.

In this work, rather than considering a point mass as in NLH1, we are considering a static matter distribution (but with a non-zero cosmological constant). Thus all functions depend only on the radial coordinate r , and the operator L_t reduces simply to $L_t = g_2(r) \partial_r$. For a given radial density profile $\rho(r)$, one has $M(r) = \int_0^r 4\pi \bar{r}^2 \rho(\bar{r}) d\bar{r}$, as previously, and our goal is to determine the unknown functions $f_1(r)$, $g_1(r)$, $g_2(r)$, $F(r)$, $G(r)$ and $p(r)$.

Substituting the above expression for $M(r)$ into the $L_t M$ equation in (35), one finds $g_2(r) \rho(r) = -g_2(r) p(r)$. Since the density and pressure must be positive in a realistic object, one immediately concludes that $g_2(r) = 0$. It is worth noting at this point that only the 'diagonal' tetrads e_i^i (no sum on i) defined in NLH1 and their inverses are non-zero. Thus, the general form of the line-element has reduced to the simple form

$$ds^2 = \frac{1}{f_1^2(r)} dt^2 - \frac{1}{g_1^2(r)} dr^2 - r^2 d\Omega^2. \quad (38)$$

Moreover, for a particle (or observer) at rest in the tetrad frame, so that its four-velocity components are $[\hat{u}^i] = [1, 0, 0, 0]$, we thus have $\dot{t} = f_1(r)$ and $\dot{r} = \dot{\theta} = \dot{\phi} = 0$. Therefore, once again, our tetrad frame defines the local laboratory of an observer at fixed spatial coordinates and the three spacelike tetrad unit vectors \hat{e}_i ($i = 1, 2, 3$) lie in the same directions as the spatial coordinate basis vectors e_μ ($\mu = 1, 2, 3$).

Since $g_2(r) = 0$, the M and $L_r g_2$ equations in (37), and the $L_t g_2$ equation in (35) yield, respectively,

$$\begin{aligned} g_1(r) &= \sqrt{1 - \frac{2M(r)}{r} - \frac{1}{3}\Lambda r^2}, \\ F(r) &= 0 \\ G(r) &= \frac{1}{g_1(r)} \left[\frac{M(r)}{r^2} - \frac{1}{3}\Lambda r + 4\pi r p(r) \right] \end{aligned} \quad (39)$$

Moreover, once $g_1(r)$ and $G(r)$ have been determined, one may immediately obtain $f_1(r)$ from the $L_r f_1$ equation in (35). Thus the solution is fully specified by the three non-zero functions $g_1(r)$, $G(r)$ and $p(r)$.

We already have an explicit expression for $g_1(r)$ in terms of known quantities, and an explicit expression for $G(r)$ that depends on the unknown function $p(r)$. The pressure profile must satisfy the $L_r p$ equation in (35), which reads

$$\frac{dp(r)}{dr} = -\frac{G(r)}{g_1(r)}[\rho(r) + p(r)]. \quad (40)$$

Combining this equation with the $G(r)$ equation in (39), one obtains the Oppenheimer–Volkov equation with a cosmological constant (Winter 2000),

$$\frac{dp(r)}{dr} = -\frac{(\rho(r) + p(r))(M(r) + 4\pi r^3 p(r) - \frac{1}{3}\Lambda r^3)}{r(r - 2M(r) - \frac{1}{3}\Lambda r^3)}, \quad (41)$$

which directly relates the pressure and density profiles of a static, spherically-symmetric perfect fluid distribution. The Oppenheimer–Volkov equation may be considered as the relativistic generalisation of the Newtonian equation of hydrostatic equilibrium (11), to which it reduces in the appropriate limits. For a given $\rho(r)$ and suitable boundary condition on the pressure, we may solve (41) to obtain $p(r)$, and hence $G(r)$.

It is worth noting that in the special case of a point mass, such that $M(r) = m = \text{constant}$, $\rho(r) = \delta(r)$ and $p(r) = 0$, one quickly finds

$$\begin{aligned} g_1(r) &= \sqrt{1 - \frac{2m}{r} - \frac{1}{3}\Lambda r^2}, \\ G(r) &= \frac{\frac{m}{r^2} - \frac{1}{3}\Lambda r}{\sqrt{1 - \frac{2m}{r} - \frac{1}{3}\Lambda r^2}}, \\ f_1(r) &= \frac{1}{\sqrt{1 - \frac{2m}{r} - \frac{1}{3}\Lambda r^2}}. \end{aligned} \quad (42)$$

The corresponding line-element (38) in this case reads

$$ds^2 = \left(1 - \frac{2m}{r} - \frac{1}{3}\Lambda r^2\right) dt^2 - \left(1 - \frac{2m}{r} - \frac{1}{3}\Lambda r^2\right)^{-1} dr^2 - r^2 d\Omega^2, \quad (43)$$

which is the Schwarzschild–de Sitter metric, as expected.

3.2.1 Boundary condition on the pressure profile

The boundary condition on $p(r)$ required to solve the Oppenheimer–Volkov equation (41) may be calculated to a high degree of accuracy by considering a series expansion of $p(r)$ about $r = 0$. For a given density profile $\rho(r)$, we can deduce a suitable form for this expansion by considering the Oppenheimer–Volkov equation in its Newtonian limit with Λ set to zero, namely

$$\frac{dp(r)}{dr} = -\frac{\rho(r)M(r)}{r^2}, \quad (44)$$

which is the Newtonian equation of hydrostatic equilibrium (11) with $\Lambda = 0$.

For the exponential density profile (6), $\rho(r) \rightarrow \text{constant}$ as $r \rightarrow 0$, and hence $M(r) \propto r^3$. From (44), we thus see that $p(r) \propto r^2$ as $r \rightarrow 0$. Thus, one may adopt a simple

Taylor expansion $p(r) = \sum_{n=0}^{\infty} p_n r^n$ about $r = 0$. For the NFW density profile (7), however, more care is required in determining the appropriate expansion, since $\rho(r) \propto 1/r$ as $r \rightarrow 0$. Therefore, in this limit, $M(r) \propto r^2$ and from (44) we have $p(r) \propto \ln r$. This logarithmic divergence at the origin must now be taken into account by instead using a power series of the form

$$p(r) = \sum_{n=0}^{\infty} \left[p_n + \tilde{p}_n \ln\left(\frac{r}{r_0}\right) \right] r^n. \quad (45)$$

For each density profile $\rho(r)$, the coefficients in the expansion for $p(r)$ can be found by substituting the corresponding series into the Oppenheimer–Volkov equation (41). These coefficients are then used to set the boundary condition on the pressure at $r = 10^{-3}r_0$, from which point (41) is numerically integrated outwards to obtain $p(r)$. As in the Newtonian case, we impose the boundary condition that the pressure itself vanishes where $dp(r)/dr = 0$.

3.2.2 Circular motion in the equatorial plane

We again consider a test particle moving along a circular path ($\dot{r} = 0$) in the equatorial plane ($\theta = \pi/2$), for which the components of the four-velocity in the tetrad frame may be written as in (29). Once again, one may obtain an expression for the 3-speed $v = \tanh \psi$ of the test particle in the tetrad frame by using the geodesic equations (30). In this case, the non-zero elements of the spin-connection (31) are again $\omega^1_{00} = \omega^0_{10}$ and $\omega^1_{22} = \omega^1_{33} = -\omega^2_{12} = -\omega^3_{13}$, where

$$\begin{aligned} \omega^1_{00} &= -\frac{g_1(r)}{f_1(r)} \frac{df_1(r)}{dr} = G(r), \\ \omega^1_{22} &= -\frac{g_1(r)}{r}, \end{aligned} \quad (46)$$

where, for ω^1_{00} , in the second equality we have used the $L_r f_1$ equation in (35).

We again find that the resulting geodesic equation for $i = 2$ is satisfied identically, that the equations for $i = 0, 3$ both reduce to $\dot{\psi} = 0$, and that the equation for $i = 1$ gives $\tanh^2 \psi = -\omega^1_{00}/\omega^1_{33}$. Thus the speed $v(r)$ of a particle in a circular orbit at coordinate radius r , as measured by a stationary observer at that radius is

$$v(r) = \sqrt{\frac{rG(r)}{g_1(r)}}. \quad (47)$$

3.2.3 Results for example density profiles

The resulting circular velocity profiles $v(r)$ and pressure profiles $p(r)$ are again indistinguishable from those plotted in Figs 2 and 3 using the Newtonian theory, and are therefore not plotted separately. Thus, even full general-relativistic corrections to are unimportant for massive objects with densities typical of galaxies and clusters (Hwang & Noh 2006).

Indeed, quite remarkably, one can show that the location of the radius $r = r_F$ at which the circular velocity $v(r)$ and the pressure $p(r)$ vanish is *identical* in the Newtonian and full general-relativistic cases, even for large densities and pressures at which general-relativistic effects become important. From (47), we see that the radius $r = r_F$ is also the point at which the radial acceleration $G(r)$ vanishes,

changing its direction from inwards for $r < r_F$ to outwards for $r > r_F$. From (40), this coincides with the radius at which $dp(r)/dr$ vanishes, which is also where $p(r)$ vanishes according to our boundary condition. Thus, evaluating the $G(r)$ -equation in (39) at $r = r_F$, one finds that

$$\frac{M(r_F)}{r_F^2} - \frac{1}{3}\Lambda r_F = 0, \quad (48)$$

which is precisely the Newtonian condition defining r_F .

Although r_F is a natural physical radius separating bound and unbound material in the galaxy or cluster, it is unclear whether $r = r_F$ can be interpreted as the *maximum size* of a massive object, since this notion depends more on the physical stability of particle orbits, rather than merely the point where the radial force on the particle vanishes.

4 GENERAL-RELATIVISTIC ANALYSIS FOR A CENTRAL POINT MASS

We now address the question of orbit stability and also consider a more realistic, time-dependent model for the background cosmological expansion, albeit at the price of modelling the central massive object as a point mass.

In NLH1, we derived the metric for a point mass m embedded in an expanding cosmological background, for spatially-flat and spatially-curved models. In the spatially-flat case, which is a reasonable description of our universe, and using non-comoving ('physical') coordinates, the metric reads

$$ds^2 = \left[1 - \frac{2m}{r} - r^2 H^2(t)\right] dt^2 + 2rH(t) \left(1 - \frac{2m}{r}\right)^{-\frac{1}{2}} dr dt - \left(1 - \frac{2m}{r}\right)^{-1} dr^2 - r^2 d\Omega^2. \quad (49)$$

Note that this metric is only applicable outside $r > 2m$. Nonetheless it is appropriate to use it for our region of interest $r \gg m$. As shown in NLH1, it is connected by a coordinate transformation to the corresponding metric derived by McVittie (1933). It is worth noting that in the special case of a de Sitter background, for which $H^2(t) = \Lambda/3$, the coordinate transformation (Arakida 2010)

$$dt = d\bar{t} - \frac{1}{\left(1 - \frac{2m}{r} - \frac{1}{3}\Lambda r^2\right)} \sqrt{\frac{\frac{1}{3}\Lambda r^2}{1 - \frac{2m}{r}}} dr. \quad (50)$$

converts the metric (49) into the standard Schwarzschild–de Sitter metric (43) (with t replaced by \bar{t}), as expected.

4.1 Radial force on a test particle

In NLH1, we also obtained an invariant expression for the force per unit mass required to keep a test particle at rest relative to the central mass m . In the spatially-flat case, this reads

$$f = \frac{\frac{m}{r^2} - rH^2(t)}{\left(1 - \frac{2m}{r} - r^2 H^2(t)\right)^{1/2}} + \frac{rH^2(t)(q(t) + 1)\sqrt{1 - \frac{2m}{r}}}{\left(1 - \frac{2m}{r} - r^2 H^2(t)\right)^{3/2}}. \quad (51)$$

In the special case of a de Sitter background, for which $H^2(t) = \Lambda/3$ and $q(t) = -1$, this reduces to the well-known result

$$f_{\text{dS}} = \frac{\frac{m}{r^2} - \frac{1}{3}\Lambda r}{\sqrt{1 - \frac{2m}{r} - \frac{1}{3}\Lambda r^2}}. \quad (52)$$

As discussed in NLH1, the Newtonian approximation to (51) in our region of interest $m \ll r \ll 1/H(t)$, and a change of sign, allows us to identify the radial force on a unit-mass test particle as simply that given in (1), namely

$$F \approx -\frac{m}{r^2} - q(t)H^2(t)r. \quad (53)$$

Thus, the force consists of the usual $1/r^2$ inwards component due to the central (point) mass m and a cosmological component proportional to r that is directed outwards (inwards) when the expansion of the universe is accelerating (decelerating).

The key difference between the general expression (53) and the special case of a de Sitter background is that the cosmological force component in the former is time-dependent. Indeed, as shown in section ??, for the standard Λ CDM concordance cosmology, the cosmological force term reverses direction at about $z \approx 0.67$, changing from an inwards directed force at high redshift (when the universal expansion is decelerating) to an outwards directed force at low redshift (as the universal expansion accelerates owing to the dominance of the dark energy component). For the standard Λ CDM concordance cosmology, the dominance of the dark energy component will increase as the universe continues to expand and so the expansion will tend to the de Sitter background model considered earlier, for which the cosmological force term is time-independent.

The time-dependence of the cosmological force term in the general case means that the radius at which the total radial force becomes zero, which marks the cut-off point for the existence of circular particle orbits, is also time-dependent. For a central point mass, this is given explicitly by

$$r_F(t) \approx \left[-\frac{m}{q(t)H^2(t)}\right]^{\frac{1}{3}}, \quad (54)$$

provided the universal expansion is accelerating, so that $q(t)$ is negative. This also marks the cut-off between gravitationally bound and unbound material, so it may be interpreted as the point separating the 'system' from the rest of the universe. Clearly, if the expansion is decelerating (i.e. for $z > 0.67$ in the Λ CDM concordance model), then the force due to the central mass m and the cosmological force are both directed inwards and so there is no radius at which the total force vanishes, and hence no natural cut-off for the size of massive objects. Thus, we see that the time-dependent cosmological force term in a general expansion will have a profoundly different effect on the formation and structure of massive objects as compared with the simple special case of a time-independent de Sitter background; in the latter case, the expression (54) reduces simply to $r_F = (3m/\Lambda)^{1/3}$.

Nonetheless, at low redshifts, where the dark energy component is dominant, we might expect that the values of r_F obtained using (54) will not differ significantly from those obtained assuming a de Sitter background. The dark energy density $\Omega_\Lambda(t) = \Lambda/[3H^2(t)]$ has the value $\Omega_{\Lambda,0} \approx 0.7$

Galaxy	Mass ($10^{11} M_{\odot}$)	P&P cut-off	$r_F(t_0)$	$r_S(t_0)$
M83	21	1.10	1.47	0.93
M81	9.2	0.75	1.12	0.70
IC 342	2	0.51	0.67	0.42
NGC 253	1.3	0.40	0.58	0.36

Table 4. Radial distances $r_F(t_0)$ and $r_S(t_0)$ in Mpc from the centre of each galaxy, assuming the galaxy to be a point mass, as compared to the empirical ‘cut-off’ radius derived by Peirani & Pacheco (‘P&P’) at which the radial velocity field vanishes; see text for details.

at the current epoch $t = t_0$ and the deceleration parameter is currently measured at $q(t_0) \approx -0.55$ (Krauss 2003). Thus, the ‘correction factor’ one should apply to our earlier results in Table 2, derived assuming a de Sitter background, is only $(-\Omega_{\Lambda,0}/q(t_0))^{1/3} \approx 1.08$, assuming that the correction required in the case of an extended central mass is approximately the same as that for a point mass.

We may compare the present-day values $r_F(t_0)$, calculated from (54), with the cut-off radii obtained in the numerical analysis by Peirani & Pacheco (2005, 2008) for specific low-redshift galaxies. This comparison is listed in Table 4, from which we see good agreement between the two approaches. It should be noted, however, that the $r_F(t_0)$ values are typically about a factor ~ 1.4 larger than the corresponding radial cut-offs derived by Peirani & Pacheco (2005, 2008). We now address this discrepancy by considering the largest *stable* circular orbits possible about the central mass.

4.2 Largest stable orbits

We have mentioned previously that the radius $r = r_F$ at which the total radial force is zero, and the circular velocity $v(r)$ also vanishes, does not necessarily correspond to the maximum possible size of the galaxy or cluster. Indeed many of the gravitationally-bound particles inside r_F may be in unstable circular orbits. A more physically meaningful ‘outer’ radius, which one may interpret as the maximum size of the object, is that corresponding to the largest *stable* circular orbit, which we denote by r_S .

The radius r_S may be determined as the minimum of the (time-dependent) effective potential for a test particle in orbit about the central mass m (Hobson, Efstathiou & Lasenby 2006). For the metric (49), we found in NLH1 that the corresponding geodesic equations lead to an equation of motion for a test particle given by

$$\ddot{r} = \frac{L^2}{r^3} \left(1 - \frac{3m}{r}\right) - \frac{m}{r^2} + rH^2(t) - \frac{2r^2H(t)H'(t)}{1 - \frac{2m}{r} - r^2H^2(t)} \dot{r} \dot{t} + \frac{H'(t)r\sqrt{1 - \frac{2m}{r}}}{1 - \frac{2m}{r} - r^2H^2(t)} \left(1 + \frac{L^2}{r^2}\right) + \frac{rH'(t)}{\sqrt{1 - \frac{2m}{r}} \left(1 - \frac{2m}{r} - r^2H^2(t)\right)} \dot{r}^2, \quad (55)$$

where L is the specific angular momentum of the test particle about the central mass m . We recall that dots denote derivatives with respect to the particle’s proper time τ ,

whereas primes denote derivatives with respect to the cosmic time t .

Expanding (55) in m and assuming a weak gravitational field and low velocities for the test particle ($\dot{t} \approx 1$, $\dot{r} \approx 0$), one obtains the approximate Newtonian expression

$$\frac{d^2r}{dt^2} \approx -\frac{m}{r^2} - q(t)H^2(t)r + \frac{L^2}{r^3}. \quad (56)$$

This is simply the Newtonian radial force expression (53) with the inclusion of a centrifugal term.

4.2.1 Analytic results

The effective potential in which the test particle moves is given by the first integral of (56) with respect to r , and so its turning points occur at the r -values for which $d^2r/dt^2 = 0$, namely the solutions of

$$q(t)H^2(t)r^4 + mr - L^2 = 0. \quad (57)$$

The two real solutions of this quartic both include the factor $\sqrt{256q(t)H^2(t)L^6 + 27m^4} \geq 0$, thus placing an upper bound on L of

$$L \leq \left[-\frac{27m^4}{256q(t)H^2(t)} \right]^{\frac{1}{6}}. \quad (58)$$

Using the maximum value of L , the radius of the largest stable circular orbit is found to be

$$r_S(t) = \left[-\frac{m}{4q(t)H^2(t)} \right]^{\frac{1}{3}}. \quad (59)$$

Comparing this expression with that for $r_F(t)$ in (54), we see that although both radii are time-dependent, they are related by a constant factor. Thus, at any epoch, the radius $r_S(t)$ of the largest stable circular orbit lies a factor $4^{1/3} \approx 1.6$ inside the radius $r_F(t)$ at which the total radial force on a test particle is zero and the circular velocity $v(r)$ vanishes. This additional ‘correction factor’ brings our estimates of the maximum possible sizes of individual galaxies into very close agreement with the cut-off radii derived by Peirani & Pacheco (2005, 2008), as shown in Table 4. For a galaxy of total mass $m \approx 10^{12} M_{\odot}$, the radius of the largest stable circular orbit at the present epoch is $r_S(t_0) \approx 0.72$ Mpc, and for a cluster of total mass $m \approx 10^{15} M_{\odot}$ we have $r_S(t_0) \approx 7.2$ Mpc. These values are consistent with the observed sizes of low-redshift galaxies and clusters respectively; only ~ 2.8 and ~ 1.4 times larger than the typical sizes quoted in Table 1. We note that in the special case of a de Sitter background, the expression (59) reduces to $r_S = (3m/(4\Lambda))^{1/3}$.

4.2.2 Numerical results

As a check on our analytical results, and to include more accurately the effect of the radius $r_S(t)$ being a function of cosmic time, we perform a numerical integration of the Newtonian equation of motion (56). In particular, we consider a test particle launched at the present cosmic epoch $t = t_0$, at an initial radius r_i from the central mass m , such that its orbit is initially circular. This corresponds to the boundary conditions $dr/dt = d^2r/dt^2 = 0$ at $t = t_0$, and thus fixes the specific angular momentum to be

$$L = \sqrt{mr_i + q(t_0)H^2(t_0)r_i^4}. \quad (60)$$

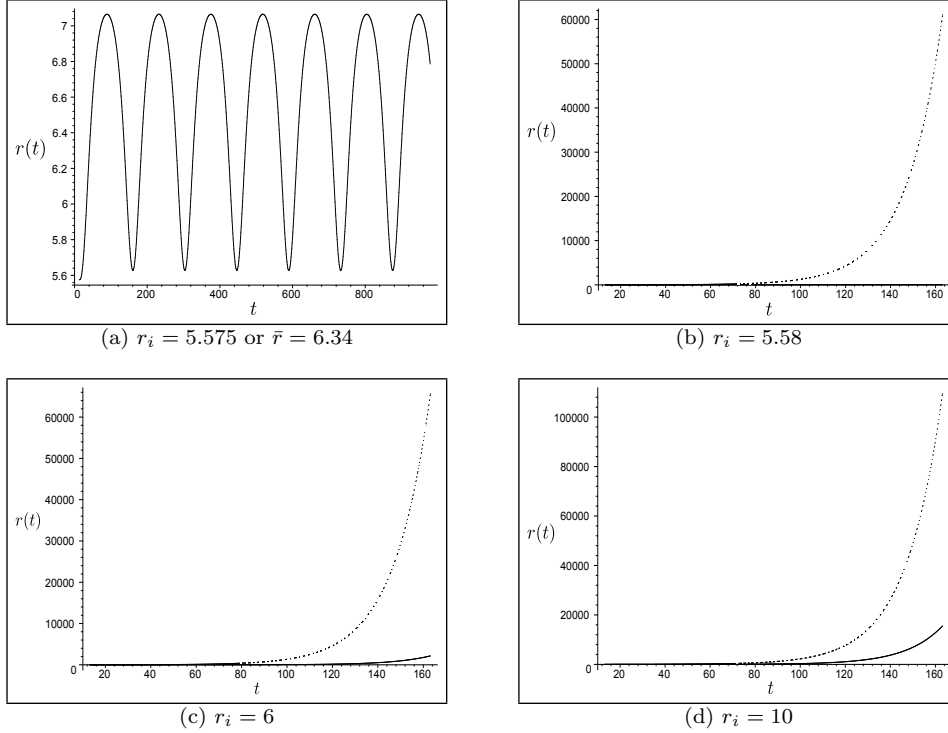


Figure 4. Trajectories $r(t)$ (in Mpc versus Gyr) of a test particle launched at the present cosmic epoch $t = t_0$, at different initial radii r_i from a central mass $m = 10^{15} M_{\odot}$, such that its orbit is initially circular. The Λ CDM concordance model universal expansion law (61) is assumed.

We take $m = 10^{15} M_{\odot}$, which corresponds to a typical large cluster, and assume a realistic expansion law $R(t)$, corresponding to the standard spatially-flat concordance model, which is given by (Hobson, Efstathiou & Lasenby 2006)

$$a(t) = \left[\frac{(1 - \Omega_{\Lambda,0})}{\Omega_{\Lambda,0}} \sinh^2 \left(\frac{3}{2} H_0 \sqrt{\Omega_{\Lambda,0}} t \right) \right]^{\frac{1}{3}}, \quad (61)$$

where $a(t) = R(t)/R_0$ is the normalised scale factor, $\Omega_{\Lambda,0} = 0.7$ and $H_0 = 70 \text{ km s}^{-1} \text{ Mpc}^{-1}$.

It is found that there is a critical initial radius, $r_{i,c} \approx 5.575 \text{ Mpc}$, above which the resulting particle trajectory expands with the universe. Physically this means that a test particle in an initial orbit of radius $r_i > r_{i,c}$ would ultimately be swept out by the universal expansion. The resulting trajectory $r(t)$ for an initial radius equal to the critical value is shown in Fig. 4(a), whereas the trajectories for larger values of r_i are shown in the other panels. One sees that for the critical value, the radius of the particle orbit oscillates about a fixed value $\bar{r} \approx 6.3 \text{ Mpc}$ that is slightly larger than r_i , which itself lies at the minimum of the oscillation. For larger values of r_i , the radius of the resulting particle orbit grows significantly with cosmic time. Nonetheless, in these latter cases, the growth of the particle orbit lags behind the universal expansion. Although this ‘lag’ becomes less pronounced for larger values of r_i , the test particle never becomes completely comoving owing to the presence of the central mass.

We note that Price (2005) has used a very similar geodesic equation to (56) to analyse the motion of an electron orbiting a central nucleus, with a slight modification to account for the dominant electrostatic force in that problem. An extension of this work is presented in Appendix ??.

4.3 Minimum density of objects

If we consider $r_S(t)$ as the maximum possible size of a massive object at cosmic time t , and make the simplifying assumption that objects are spherically-symmetric and have constant density, then the condition (59) shows that there exists a time-dependent minimum density for objects, given by

$$\rho_{\min}(t) = \frac{3m}{4\pi r_S^3(t)} = -\frac{3q(t)H^2(t)}{\pi G}, \quad (62)$$

where in the last equality we have reinserted a factor of G to convert back to SI units. It should be noted that, since (59) is valid only for $q(t) < 0$ (accelerating expansion), then this restriction also applies to (62). For $q(t) > 0$, $\rho_{\min}(t)$ vanishes.

We point out that in the special case of a de Sitter background, Nowakowski, Sanabria & Garcia (2002) calculate the minimum density for objects to remain gravitationally bound to be $\rho_{\min} = \Lambda/(4\pi G)$. This is a factor of 4 smaller than our result for a de Sitter background. It does however, correspond to what we would obtain by defining $\rho_{\min}(t) = 3m/(4\pi r_F^3)$, with $r_F = (3m/\Lambda)^{1/3}$. Since r_F corresponds only to the *theoretical* maximum size of an object, and not the true maximum *attainable* size given by $r_S = (3m/(4\Lambda))^{1/3}$, we believe our estimate of the minimum density to be more realistic.

Using (62) one finds that, at the present cosmic epoch, $\rho_{\min}(t_0) \sim 4 \times 10^{-26} \text{ kg m}^{-3}$, which should be compared with the present-day critical density $\rho_{\text{crit},0} \sim 9 \times 10^{-27} \text{ kg m}^{-3}$ required for the universe to be spatially-flat. Indeed, since at any cosmic epoch, $\rho_{\text{crit}}(t) = 3H^2(t)/(8\pi G)$, one has

simply

$$\frac{\rho_{\min}(t)}{\rho_{\text{crit}}(t)} = -8q(t), \quad (63)$$

provided $q(t) < 0$. Alternatively, since the average matter density $\rho_m(t) = \Omega_m(t)\rho_{\text{crit}}(t)$, the minimum fractional density contrast $\delta_{\min}(t) \equiv [\rho_{\min}(t) - \rho_m(t)]/\rho_m(t)$ of a matter fluctuation at cosmic time t is

$$\delta_{\min}(t) = - \left[1 + \frac{8q(t)}{\Omega_m(t)} \right]. \quad (64)$$

Inserting the present-day values $\Omega_{m,0} \approx 0.3$ and $q_0 \approx -0.55$, one finds $\delta_{\min}(t_0) \approx 14$.

The above expressions and values are, of course, rather approximate. In particular, our r_S values have been calculated assuming a central mass point rather than an extended mass and realistic astrophysical objects do not have uniform densities. Nonetheless, the above arguments can be taken as an indication of the *existence* and rough order of magnitude of such a minimum density. Calculated accurately, this minimum density should correspond to that required for any structure formation at all to occur at a given cosmic time t during an accelerated expansion phase of the universe. We leave this as a topic for future research.

4.4 Comparison with previous studies

Balaguera-Anol3nez, B3hmer & Nowakowski (2005) and Nowakowski & Balaguera-Anol3nez (2006) have previously used the Schwarzschild de Sitter metric (43) to find expressions for (what we call) r_F and r_S in the special case of a de Sitter background universe.

It is worth noting that they were able to use a more traditional method to find r_F and r_S , since the Schwarzschild de Sitter metric is static. In such cases, one can combine the resulting geodesic equations into an ‘energy’ equation of the form $\frac{1}{2}\dot{r}^2 + U_{\text{eff}}(r) = E$, where E is the total energy of the particle per unit rest mass and one can read off the effective potential $U_{\text{eff}}(r)$. For the Schwarzschild de Sitter metric (43), this is given by

$$U_{\text{eff}}(r) = -\frac{m}{r} - \frac{1}{6}\Lambda r^2 + \frac{L^2}{2r^2} - \frac{mL^2}{r^3}. \quad (65)$$

The value of r_F is then simply the location of the minimum of $U_{\text{eff}}(r)$ with $L = 0$, which immediately leads to an expression for r_F which agrees precisely with our result (54) in the special case of a de Sitter background. The value of r_S is the location of the minimum of $U_{\text{eff}}(r)$ with $L = L_{\text{max}}$, where L_{max} is maximum value of L for which $U_{\text{eff}}(r)$ possesses a minimum. In the limits $L \gg m$ and $\Lambda \ll 1$ adopted by these authors, the resulting expression for r_S agrees with our result (59) in the de Sitter case.

This approach should be contrasted with the derivation in NLH1 of the equation of motion (55). The latter is more complicated owing to the dependence of the metric (49) on the cosmic time t , which prevents one arriving at an ‘energy’ equation. Nonetheless, we note that in the special case of a de Sitter background, the equation of motion (55) reduces to

$$\ddot{r} = -\frac{m}{r^2} + \frac{1}{3}\Lambda r + \frac{L^2}{r^3} \left(1 - \frac{3m}{r} \right). \quad (66)$$

The first integral of this equation then immediately yields an ‘energy’ equation with the effective potential (65).

We further note that Sussman & Hernandez (2003) also obtained the factor $r_F/r_S \approx 1.6$ for a de Sitter background, but individual values of r_F and r_S are greater than ours by a factor of ~ 10 for galaxies and ~ 3 for clusters. Their approach deviates significantly from our work and that of Balaguera-Anol3nez, B3hmer & Nowakowski (2005) and Nowakowski & Balaguera-Anol3nez (2006), since they model galaxies and clusters as dark matter haloes in equilibrium with a static ‘ Λ -field’, rather than simply as point masses. It is possible that, by taking the spatial extent of the central object into account, we may close this small discrepancy between our results, but we leave this as a topic for future research. We point out that Sussman & Hernandez obtain the values of r_F and r_S by numerically integrating two coupled differential equations, so no analytical results are given in their work.

5 PHANTOM ENERGY AND THE ‘BIG RIP’

We have thus far considered dark energy only in the form of a cosmological constant, for which the equation-of-state parameter $w = -1$. This is well supported by observations, but more generic dark energy models allow for w to differ from -1 , and even to vary with cosmic epoch. In any case, $w = -1$ is usually considered as the lower-limit, since a dark energy ‘fluid’ with $w < -1$ violates all the relativistic energy conditions. Nonetheless, this has not deterred some theorists from considering the cosmological consequences of a dark energy component with a constant equation-of-state parameter $w < -1$, which is often termed ‘phantom-energy’ (Caldwell 2002). We now consider the effect on massive objects of a cosmological expansion driven by phantom energy.

5.1 The Big Rip

As shown by Caldwell, Kamionkowski & Weinberg (2009), the most profound consequence of phantom energy is that it leads to a ‘Big Rip’ in the far future, at which the universe scale factor and Hubble parameter become singular.

To explain this, for simplicity let us consider a spatially-flat model, which is a good approximation to our universe. The Friedmann equation governing the time evolution of the normalised scale factor $a(t)$, assuming negligible radiation energy density, is

$$H^2(t) = H_0^2 \left[\Omega_{m,0} a^{-3}(t) + (1 - \Omega_{m,0}) a^{-3(1+w)}(t) \right], \quad (67)$$

where $H(t) = a'(t)/a(t)$, $\Omega_{m,0} \approx 0.3$ is the present-day matter density parameter and the current value of the Hubble parameter is taken to be $H_0 \approx 70 \text{ km s}^{-1} \text{ Mpc}^{-1}$.

At late times the second term on the right-hand side, relating to dark energy, dominates over the first, relating to matter. Writing $1 + w$ as $-|1 + w|$, the Friedmann equation may be written as $H^2(t) = H_0^2 (1 - \Omega_{m,0}) a^{-3|1+w|}(t)$. Solving for the normalised scale factor then gives

$$a(t) = \left[\frac{2}{3|1+w| \left(H_0 \sqrt{1 - \Omega_{m,0}} (t_0 - t) + \frac{2}{3|1+w|} \right)} \right]^{\frac{2}{3|1+w|}}.$$

(68)

One sees immediately that $a(t)$, and hence $H(t)$, diverges at a finite time $t = t_{\text{rip}}$ in the future that satisfies

$$t_{\text{rip}} - t_0 \approx \frac{2}{3|1 + w|H_0\sqrt{1 - \Omega_{m,0}}}. \quad (69)$$

If $w = -\frac{3}{2}$, for example, the time remaining for the universe before the Big Rip is ~ 22 Gyrs.

5.2 Times at which objects become unbound

Since $H(t)$ becomes infinite at $t = t_{\text{rip}}$, then so does the cosmological component of the radial force (53) on a test particle in the vicinity of a central mass. Moreover, since $q(t) < 0$ for the accelerating expansion during phantom-energy dominance, this force is directed outwards, away from the central mass. Thus, by the time of the Big Rip, all massive objects will have been ripped apart.

We now consider the time before the Big Rip that this occurs for an object of a mass m and size r . Note that we only perform a rough calculation due to our simplifying assumptions. For example, we assume the mass to be concentrated at the centre of the object, as in a standard Newtonian framework. We then specifically calculate the time at which a particle at the edge of the object becomes gravitationally unbound from it; that is when the inwards force component of magnitude m/r^2 , due to the central mass, is balanced by the outwards component of magnitude $|q(t)H^2(t)r|$ due to the (accelerating) cosmological expansion. Note that this is not the same as calculating the time at which the point mass itself is ripped apart, which we are unable to evaluate due to the singularity in our model at $r = 2m$. Nonetheless, it is the time at which the object ceases to exist in its current state and begins to be ripped apart, as layers of it gradually peel off as the cosmological force increasingly dominates over the gravitational force. Since the particle is at a distance $r \gg m$, the physical singularity in our model at $r = 2m$ does not affect the result.

At late times, substituting $a(t)$ from (68) into the appropriate form of the Friedmann equation $H^2(t) = H_0^2(1 - \Omega_{m,0})a^{-3|1+w|}(t)$, one finds

$$H^2(t) = \left(\frac{2}{3|1+w|\tilde{t}} \right)^2, \quad (70)$$

where $\tilde{t} = t_{\text{rip}} - t$ is the time before the Big Rip. It is worth noting that this result is independent of both H_0 and $\Omega_{m,0}$. Moreover, we see that at late times the deceleration parameter tends to the constant value

$$q(t) \rightarrow -\frac{1}{2}|1 + 3w|. \quad (71)$$

Thus the time before the Big Rip at which the total radial force (53) on a particle at the surface of an object of mass m and radius r vanishes is given by

$$\tilde{t} \approx \frac{\sqrt{2|1 + 3w|}}{3|1 + w|} \sqrt{\frac{r^3}{m}}. \quad (72)$$

Although this is only an approximate result, based on the Newtonian force expression (53), it remarkably matches Caldwell's approximate expression precisely, despite the latter being derived in a rather different manner based on energy arguments. This could be merely a coincidence, but to

Object	m	r	\tilde{t}
Galaxy cluster	$10^{15} M_{\odot}$	5 Mpc	9.3 Gyr
Milky Way	$5.8 \times 10^{11} M_{\odot}$	15 kpc	69.9 Myr
Solar System	M_{\odot}	150×10^9 m	3.6 months
Earth	6×10^{24} kg	6371×10^3 m	25.2 mins

Table 5. The times \tilde{t} before the Big Rip at which objects with a given mass m and size r are expected to be ripped apart, assuming a phantom energy equation-of-state parameter $w = -3/2$. In this case, the time until the Big Rip is $t_{\text{rip}} - t_0 \approx 22$ Gyr.

determine the true extent to which our two approaches may in fact be parallel requires further thought. We leave this for future research.

For $w = -3/2$, the times \tilde{t} before the Big Rip that specific objects of mass m and size r are expected to rip apart are given in Table 5. It is assumed (admittedly, rather implausibly) that, as the universe evolves, the objects do not accrete any additional mass, that their size remains fixed at the present-day value until they are ripped apart, and that non-gravitational binding forces are negligible.

6 CONCLUSIONS

In Nandra, Lasenby & Hobson (2011) we derived the metric for a point mass m embedded in an expanding cosmological background, for both spatially-flat and spatially-curved universes. We also derived the corresponding invariant expression in each case for the force required to keep a test particle at rest relative to the central mass. In this paper, we have presented some important astrophysical consequences of this work, focussing on the effect of an expanding universe on massive objects on the scale of galaxies and clusters.

For a spatially-flat universe in the Newtonian limit, the force on a test particle at a distance r from a point mass m consists of the usual time-independent $1/r^2$ inwards component due to the central mass and a time-dependent cosmological component proportional to r that is directed outwards (inwards) when the expansion of the universe is accelerating (decelerating). It is immediately clear, therefore, that the effect of an expanding universe on a massive object is profoundly different if the expansion is accelerating as opposed to decelerating. In the latter case, the force on a constituent particle of a galaxy or cluster is attractive for all values of r and tends gradually to zero as $r \rightarrow \infty$ (for any sensible radial density profile), with no definite cut-off. In the former case, however, the force on a constituent particle (or equivalently its radial acceleration) *vanishes* at a some *finite* radius r_F (say), beyond which the net force becomes repulsive. This is also the radius of the largest possible circular orbit about the central mass. This suggests that an accelerating cosmological expansion should set a *maximum size*, dependent on mass, for galaxies and clusters.

Although our force expression accommodates a realistic dynamical expanding background cosmology, it comes at the price of modelling the central massive object as a point mass. In reality, it is more appropriate to model galaxies or clusters as extended objects having some density profile. We consider this in the special case of a de Sitter back-

ground, which simplifies matters considerably. In this case, the expansion is always accelerating and the analysis can be performed in an entirely static manner with the inclusion of a non-zero cosmological constant. Although the de Sitter background is not an accurate representation of our universe, the standard cosmological model is dominated by dark-energy in a form consistent with a simple cosmological constant, which is driving the current observed accelerated phase of expansion.

We calculate the value of r_F in this case for spherically-symmetric matter distributions with an exponential and NFW radial density profile, respectively, using Newtonian theory, linearised general-relativity and the full non-linear Einstein field equations. The three methods give indistinguishable results for objects with masses and sizes typical of galaxies and clusters, as might be expected. More surprising, perhaps, is that one can show analytically that the location of $r = r_F$ is identical in the Newtonian and full general-relativistic cases. For clusters we find $r_F \sim 10.5\text{--}12.0$ Mpc and for galaxies we find $r_F \sim 1.06\text{--}1.20$ Mpc, which, as maximum sizes, are compatible with the sizes of 5 Mpc and 0.26 Mpc respectively. In addition, for galaxies our values for r_F agree well with the typical radius at which the radial velocity field in the neighbourhood of nearby galaxies vanishes, as inferred by Peirani & Pacheco (2005, 2008) from recent observations of stellar velocities in such objects. In the Newtonian and fully general-relativistic analyses, we include the effects of pressure and derive the radial pressure profile $p(r)$ in the central object. We find that $dp(r)/dr$ also vanishes precisely at $r = r_F$, as does $p(r)$ itself according to our boundary condition. In the Newtonian case, we obtain analytical results for pressure and temperature profiles in the case of an NFW density profile.

The key difference between a general expression and the special case of a de Sitter background is that, in the former, the cosmological component of the radial force on a test particle is time-dependent. This means that the radius r_F at which the total radial force becomes zero, which marks the cut-off point for the existence of circular particle orbits, is also time-dependent. In particular, for the standard Λ CDM concordance cosmology, there is no finite radius at which the total force vanishes, and hence no natural cut-off for the size of massive objects, during the decelerating phase prior to $z \approx 0.67$. Nonetheless, returning to our model of the central massive object as a point mass, we find that at low redshifts, where the dark energy component is dominant, the values of r_F obtained do not differ significantly from those obtained assuming a de Sitter background.

For a general cosmological expansion, the radius r_S of the largest stable circular orbit is also time-dependent, but we find that at any cosmic epoch it is simply a factor $4^{1/3} \approx 1.6$ smaller than r_F . It is also perhaps a more appropriate measure than r_F for the maximum possible size of an object of mass m . Indeed it is encouraging that we find the factors r_S/r_T at the present time for both galaxies and clusters to be close to 1; we obtain ~ 2.8 and ~ 1.4 respectively. We also obtain an approximate expression, dependent only on cosmological parameters, for the minimum density of an object for it to remain gravitationally bound at a given cosmic epoch.

Finally, we also consider the future effect on massive objects of cosmological expansion driven by dark energy with

an equation-of-state parameter $w < -1$, termed phantom energy. In such a model the universe is predicted to end in a ‘Big Rip’ at a finite time in the future at which the scale factor and the Hubble parameter become singular. Using our radial force equation, we obtain an expression for the time prior to the Big Rip that an object of a given mass and size will become gravitationally unbound. Remarkably, this is found to agree precisely with the approximate expression derived by Caldwell using a rather different approach based on energy arguments.

ACKNOWLEDGEMENTS

RN is supported by a Research Studentship from the Science and Technology Facilities Council (STFC).

REFERENCES

- Arakida H., 2009, *New Astron.*, 14, 264
 Balaguera-Anol3nez A., B3hmer C.G., Nowakowski M., 2005, *Class. Quant. Grav.*, 23, 485
 Binney J., Tremaine S., 2008, *Galactic Dynamics*, 2nd Ed., Princeton University Press
 Caldwell R.R., Kamionkowski M., Weinberg N.N., 2003, *Phys. Rev. Lett.*, 91, 071301
 Caldwell R.R., 2002, *Phys. Lett. B*, 545, 23
 Carmeli M., Kuzmenko T., 2001, in Wheeler J.C., Martel H., eds, *AIP Conf. Proc. Vol. 586, 20th Texas Symp. on Relativistic Astrophysics*. Am. Inst. Phys., New York, p. 316
 Carroll S.M., 2001, *Living Rev. Relativity*, 4, 1
 Crain R.A., McCarthy I.G., Schaye J., Frenk C.S., Theuns T., 2010, arXiv:1011.1906v1
 Davis T.M., Lineweaver C.H., Webb J.K., 2003, *American Journal of Physics*, 71, 358
 Faraoni V., Jacques A., 2007, *Phys. Rev. D*, 76, 063510
 Fleenor M.C., Rose J.A., Christiansen W.A., 2006, *Astron. J.*, 131, 1280
 Garnavich P.M. et al., 1998, *ApJ*, 493, L53
 Henley D.B., Shelton R.L., Kwak K., Joung M.R., Mac Low M.-M., 2010, *ApJ*, 723, 935
 Hwang J.-C., Noh H., 2006, *MNRAS*, 367, 1515
 Hobson M.P., Efstathiou G., Lasenby A.N., 2006. *General Relativity*, Cambridge University Press, New York
 Hubble E., 1929, *Proc. Natl. Acad. Sci.*, 15:3, 168
 Karachentsev I.D., 2005, *The Astronomical Journal*, 129, 178
 Klypin A., Zhao H.S., Somerville R.S., 2002, *ApJ*, 573, 597
 Kratochvil J., Linde A., Linder E.V., Shmakova M., 2004, *JCAP*, 0407, 001
 Krauss L.M., 2003, *ApJ*, 596, L1
 Lahav O., Lilje P.B., Primack J.R. Rees M.J., 1991, *MNRAS*, 251, 128
 Lasenby A., Doran C., Gull S., 1998, *Phil. Trans. R. Soc. Lond. A*, 356, 487
 Lema3tre G., 1933, *Ann. Soc. Sci. Brux.*, A53, 51
 Lynden-Bell D., 1967, *MNRAS*, 136, 101
 Lynden-Bell D., 1981, *The Observatory*, 101, 111
 Matos T., Nu3nez D., Sussman R.A., 2004, *Class. Quant. Grav.*, 21, 5275

- McCauley J.L., 1997, *Classical Mechanics: Transformations, Flows, Integrable and Chaotic Dynamics*, Cambridge University Press, Cambridge
- McVittie G.C., 1933, *MNRAS*, 93, 325
- Misner C.W., Thorne K.S., Wheeler J.A., 1973, *Gravitation*, Freeman & Co., New York
- Nandra R., Lasenby A., Hobson M., 2011, *MNRAS*, 422, 2931
- Navarro J., Frenk C., White S., 1996, *ApJ*, 462, 563
- Nowakowski M., Sanabria J.-C., Garcia A., 2002, *Phys. Rev. D*, 66, 023003
- Nowakowski M., Balaguera-Anolín A., 2006, in Alimi J.-M., Füzfa A., eds, *AIP Conf. Proc. Vol. 861, Albert Einstein Cent. Int. Conf. Am. Inst. Phys.*, New York, p. 1001
- Peirani S., de Freitas Pacheco J.A., 2005, *New Astronomy*, 11, 4, 325
- Peirani S., de Freitas Pacheco J.A., 2008, *A&A*, 488, 3, 845
- Price R.H., 2005, arXiv:gr-qc/0508052v2
- Riess A.G. et al., 2004, *ApJ*, 607, 665
- Roncarelli M., Ettori S., Dolag K., Moscardini L., Borgani S., Murante G., 2006, *MNRAS*, 373, 1339
- Sandage A., 1986, *ApJ*, 307, 1
- Straumann N., 2002, arXiv:gr-qc/0208027v1
- Sussman R.A., Hernandez X., 2003, *MNRAS*, 345, 871
- Tolman R.C., 1934, *Proc. Nat. Acad. Sci.*, 20, 169
- Tormen G., Bouchet F.R., White S.D.M., 1997, *MNRAS*, 286, 865
- Vikhlinin A., Kravtsov A., Forman W., Jones C., Markevitch M., Murray S.S., Van Speybroeck L., 2006, *ApJ*, 640, 691
- Weinberg S., 1989, *Rev. Mod. Phys.*, 61, 1
- Winter D., 2000, *J. Math. Phys.*, 41, 5582

APPENDIX A: AN ATOM'S 'ALL-OR-NOTHING' BEHAVIOUR

Price (2005) has analysed the motion of an electron of mass m_e orbiting a central nucleus using the weak field, low velocity geodesic equation (56). For this model, he has shown that it is appropriate simply to replace the m/r^2 gravitational force in (56) with $C/r^2 = QQ'/(4\pi\epsilon_0 m_e r^2)$, where QQ' is the product of the nuclear and electron charges. Price questions whether or not the electron eventually takes part in the cosmological expansion; that is, does the electron follow a trajectory of constant 'physical' coordinate r (no atomic expansion) or of constant comoving coordinate \hat{r} (full cosmological expansion of the atom), or does the electron do something 'in-between'? Using the model expansion law $a(t) = 1 + t^2 \tanh(t)$, where $a(t) = R(t)/R(t_0)$, and launching the test particle in a momentarily circular orbit with $r = 1$ (arbitrarily) at $t = 0$, $(dr/dt)_{t=0} = (d^2r/dt^2)_{t=0} = 0$ and thus $C = L^2$, Price finds that there is a critical value of the electron's specific orbital angular momentum $L \approx 3.46$ that determines an 'all-or-nothing' behaviour: that is a weakly bound atom ($L \leq 3.46$) will eventually begin to stretch in size and participate wholly in cosmological expansion ('all' behaviour), whereas a tightly bound atom ($L > 3.46$) will eventually ignore the cosmological expansion and settle into a circular orbit of fixed 'physical' radius ('nothing' behaviour). We have been able to reproduce Price's results using his expansion law and initial conditions.

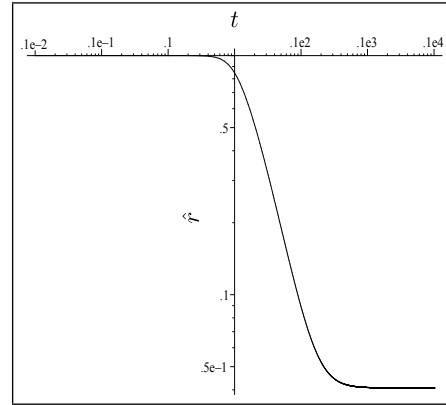


Figure A1. The cosmological radius $\hat{r} = r/a(t)$ of an electron orbit around a central nucleus for the critical value $L = 3.46$ of the electron's specific orbital angular momentum.

Fig. A1 shows the comoving radius of the electron orbit as a function of cosmic time t for the critical value $L = 3.46$, which shows an apparent plateau at late times that Price interpreted as 'all' behaviour.

Closer inspection of the 'all' behaviour reveals, however, a subtlety that was not addressed previously. The apparent plateau in Fig. A1 is not actually flat at all; rather \hat{r} continues to decrease at late times but at a much slower rate than previously. For this value of L , the atom, in fact, exhibits only a 'something' behaviour. Fig. A2 shows instead the 'physical' radius r of the electron's orbit, together with the universal scale factor $a(t)$. It then becomes clear that the atom does indeed expand forever, but at a rate that increasingly lags behind the cosmological expansion for $L = 3.46$. As we decrease L , for even less tightly bound atoms, the amount by which the electron's expansion lags behind the cosmological expansion decreases. Eventually, for $L \leq 0.1$, the two expand at the same rate and the behaviour changes from 'something' to 'all'.

This paper has been typeset from a $\text{\TeX}/\text{\LaTeX}$ file prepared by the author.

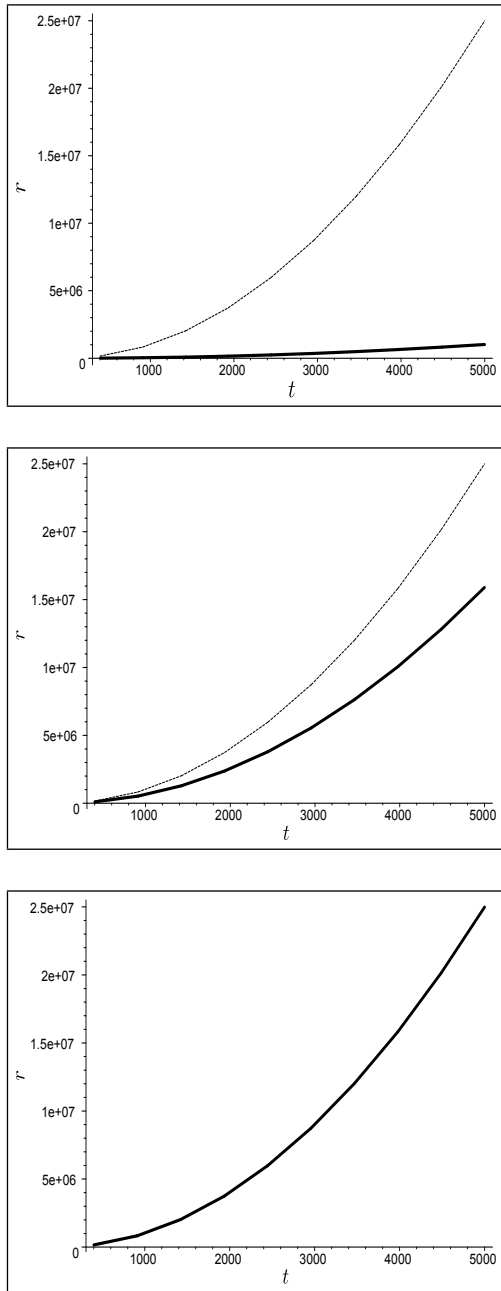


Figure A2. The ‘physical’ radius r (bold line) of an electron orbit around a central nucleus for different values of the electron’s specific angular momentum: $L = 3.46$ (top), $L = 2.5$ (middle), $L = 0.1$ (bottom). The scale factor $a(t)$ is shown as the dashed line.